Constraining the Venus interior structure with future VERITAS measurements of the gravitational atmospheric loading

Gael Cascioli[1,2,3], Joe P. Renaud[3,4], Erwan Mazarico[3], Daniele Durante[5], Luciano Iess[5], Sander Goossens[3] and Suzanne Smrekar[6]

Abstract

The complex dynamics of the Venus atmosphere produces a periodic mass redistribution pattern which creates a time variable modulation of the gravity field of Venus. Said gravity signal depends on the net transport of mass across the globe and on the response of the solid body to the normal loading of its crust imparted by the atmosphere. In this work, we explore the possibility of measuring this phenomenon with VERITAS, a NASA Discovery-class mission. By simulating the gravity science experiment, we explore the possibility of measuring the response of Venus to the atmospheric loading, parametrized by the loading Love numbers (k_l'), and assess the dependency of these parameters on fundamental interior structure properties. Using the most recent models of Venus' interior, we compute the Venus Love numbers in a compressible viscoelastic setting and compare them with the predicted uncertainty of the VERITAS measurements. We show that VERITAS will measure k_2' at the 4% level and that this measurement could possibly help to distinguish between different equally plausible interior structure models, especially allowing to distinguish different rheological laws. We also show that a measurement campaign such as the VERITAS gravity science investigation has the potential of measuring k_2' not only at the loading forcing frequency, but also at the tidal frequency, ultimately providing a way to probe the response of the planet at different forcing periods.

[1] Corresponding author gael.cascioli@umbc.edu
[2] University of Maryland, Baltimore County, MD 21250
[3] NASA Goddard Space Flight Center, Greenbelt, MD 20771
[4] University of Maryland, College Park, MD 20742
[5] Sapienza University, Rome, Italy
[6] NASA Jet Propulsion Laboratory, Pasadena, CA 91109

1. Introduction

The next decade will be the decade of Venus. The missions recently selected by NASA and ESA (VERITAS, DAVINCI, and EnVision) aim to radically advance our understanding of Earth's neighboring planet. The questions of the scientific community pushing for renewing and updating the available datasets of Venus are compelling. For instance, Venus' interior structure has not been probed by a planetary mission since the conclusion of the Magellan mission in 1994. The datasets gathered by Magellan were revolutionary for the time, but now fall far behind, in terms of accuracy, resolution, and detail when compared to our knowledge of the other terrestrial bodies of the Solar System and the capability of current planetary missions' instrumentation. Venus and its remaining mysteries represent a central comparative case towards understanding the key elements determining (exo)planetary habitability (Kane et al., 2019; Way et al., 2016).

VERITAS (Venus Emissivity, Radio science, InSAR, Topography, And Spectroscopy; Smrekar et al., 2022) will conduct a gravity science investigation mainly devoted to the measurement of the gravity field, the solid body tidal response, and the rotational state of Venus, ultimately aimed at refining our understanding of the interior structure of the planet. The radio tracking system of VERITAS, enabling the gravity science experiment, is designed to deliver a sensitivity improved by orders of magnitude with respect to what NASA's Magellan was able to achieve. This improved sensitivity gives access to dynamical effects already present in the Magellan data but below the noise floor. As recently pointed out by Goossens et al. (2018) and Bills et al. (2020) the reduced noise floor would reveal, in the tracking data, the gravitational signature of the complex interplay between the thick Venusian atmosphere and the solid planetary body, through the mechanism of the atmospheric thermal tides. This global atmospheric mechanism manifests itself (gravitationally speaking) both directly, due to the net gravity anomaly produced by the displacement of atmospheric mass, and indirectly, with the solid planet's response to this moving gravitational normal load on its surface. Petricca et al. (2022) showed that the gravitational response to the atmospheric loading strongly depends on the interior properties of the planet, through the loading Love numbers, and suggested that its measurement will provide significant constraints on the inversion of Venus' interior structure.

It has previously been shown that VERITAS gravity measurements will be sensitive to this phenomenon (*Cascioli et al.*(2021)). This previous study, however, concentrated in demonstrating that an imperfect knowledge of the atmospheric thermal tides would not compromise the scientific objectives of VERITAS. Here, we change our perspective and investigate whether VERITAS could take advantage of its sensitivity to the atmospheric dynamics. We assess the capability and quality of a measurement of the Venus' response to the atmospheric loading (*i.e.*, the loading Love numbers k_l') and evaluate the importance of these measurements in producing additional constraints on the interior structure of Venus.

Precise knowledge of Venus' interior structure is essential to solving major outstanding questions about the evolution of rocky planets. Key questions include: What is the composition of initial accretionary material? Why does Venus lack a dynamo-driven magnetic field? How did early differentiation processes affect core size and state and mantle structure? Absent Earth-like plate tectonics, what is Venus' geodynamic system? Specifically, how do interior structure and heat loss couple to observable surface geology and atmospheric composition and evolution?

The composition, phase, and convective state of core govern how much heat is lost from the core into the mantle. A better knowledge of the core and the core-mantle boundary is needed to discriminate between hypotheses to explain why Venus has no measurable dynamo today (Jacobson et al., 2017). Nimmo (2002) proposes that Venus lacks core convection and a dynamo because heat is not lost rapidly enough through the mantle and lithosphere due to the absence of plate tectonics. O'Rourke et al. (2018) hypothesize that Venus could have a basal magma ocean that suppresses heat flow from the core. The nature of the core mantle boundary and core heat loss is also critical for understanding the origin of the ~10 large mantle plumes that appear active today (*e.g.*, S. E. Smrekar & Sotin, 2012). An additional major question is why Venus exhibits two scales of mantle plumes. The large volcanic rises are similar in scale and surface features to Earth's mantle plume features, *e.g.*, Hawaii. But hundreds of smaller scale features called coronae, with an average diameter of a few hundred kilometers, also occur. Could they also originate at the core-mantle boundary (Jellinek, 2002), or do they require an additional, shallower transition zone or interface? Why are they unique to Venus?

On Earth, plate tectonics shapes Earth's long-term climate and volatile budget via volcanic outgassing and recycling of material into the mantle via subduction. An essential question for Venus is whether or not surface volcanism is largely constant over time or if there was a past 'catastrophic' event. Catastrophic resurfacing motivates the hypothesis of episodic plate tectonics (or mobile lid convection), which would allow for past periods of mobile lid activity and high heat flow, leading to a current period of stagnant lid convection and lower heat flow. Mantle viscosity and lithospheric strength, a function of mantle heat flow, are the driving parameters for mobile lid versus stagnant lid behavior, as well as for volcanism. Many have advocated for an episodic mobile lid (*e.g.*, Rolf et al., 2018; Weller & Kiefer, 2020), though other styles of a stagnant lid convection are possible, such as sluggish lid (Davaille et al., 2017) or squishy lid regimes (Lourenço et al., 2020), incorporating evidence for likely active subduction and volcanism. Constraints on mantle viscosity and structure are needed to refine these hypotheses and discriminate between geodynamic models.

The aim of this work is to demonstrate that VERITAS will be able to measure the Venus loading Love numbers and to assess the importance of their retrieved values for gaining more information on the planet's interior structure. To this end, we review the latest published models of the Venus deep interior and use them to compute the range of expected values of the tidal and loading Love numbers of Venus, under different assumptions regarding core state, radius, mantle viscosity, and temperature profile. We simulate the mission scenario embedding several sources of possible model errors to determine VERITAS' sensitivity to the load Love numbers in a robust manner. Finally, we assess the relevance of these estimates for providing improved constraints on Venus' interior.

This manuscript is structured as follows: in Section 2 we discuss the gravitational signature of the atmospheric thermal tides and their modelling; in Section 3 we detail the methodology for computing the tidal and loading Love numbers of Venus and discuss their relation to the interior structure; Section 4 follows with a discussion on how the loading Love numbers can be measured by VERITAS and the description and results of the numerical simulations used to assess the sensitivity to these parameters; Section 5 comments on the implication of VERITAS measurements in terms of Venus' interior structure constraints; and finally Section 6 provides concluding remarks.

2. Gravitational signature of atmospheric thermal tides

Venus rotates in a retrograde direction with a period of ~243 days and has an orbital period of ~224 days. The difference between these two periods gives rise to a solar day of duration T_S = 116.752 days. The radiative input of the Sun on the atmosphere determines a hotter zone in proximity of the sub-solar point and a cooler zone in the opposite hemisphere. This temperature dichotomy of the atmosphere gives rise to a mass transport phenomenon known as an atmospheric thermal tide. The atmosphere near the sub-solar point is hotter than the average and thus expands (*i.e.*, the density is lower) while on the opposite hemisphere the contrary occurs (Dobrovolskis & Ingersoll, 1980; Gold & Soter, 1971). Thus, in principle, the solar input creates a stable atmospheric thermal tide that rotates with respect to the body-fixed frame with a period equal to the solar day. The phenomenon, however, is more complex than this simple description, as the pressure field strongly depends on the topography of the Venus surface (see Figure 1). Moreover, the total gravitational perturbation is affected by other small-scale atmospheric waves. However, the contribution of the planetary-scale thermal tides to the gravity field is by far the largest (Bills et al., 2020; Petricca et al., 2022). The total gravitational signal is due to both the direct contribution (net transport of mass) and the modification of the solid body gravitational potential due to atmospheric loading on the surface (Wahr et al., 1998). To correctly compute the gravitational signal due to the atmospheric dynamics, then, a precise global circulation model (GCM) is needed. In this work we use the same atmospheric gravity field model as Goossens et al. (2017, 2018), derived from pressure fields simulations by Garate-Lopez et al. (2018). Since we are interested in the estimation of the low-degree (*i.e.*, large spatial scale) loading Love numbers, we assume that the total gravitational perturbation is only due to thermal tides. Admittedly the current Venus GCMs are not necessarily tailored to deliver a fine description of the surface pressure anomalies, the main quantity driving our modeling of the gravitational signal of the tides, mainly because of the scarcity of in-situ measurements and of the strong effect that poorly constrained parameters such as the shortwave heating rate of the lower haze below the cloud deck, the ground thermal inertia or the cloud top altitude at high latitudes can have on the low atmosphere dynamics (*e.g.*, Garate-Lopez & Lebonnois, 2018; Navarro et al., 2023).

Indeed, in our work we rely on the GCM predictions but try to mitigate the model dependency of the results by exploring different perturbed realizations of the surface pressure fields (see Section 4.1), allowing for a more robust interpretation.

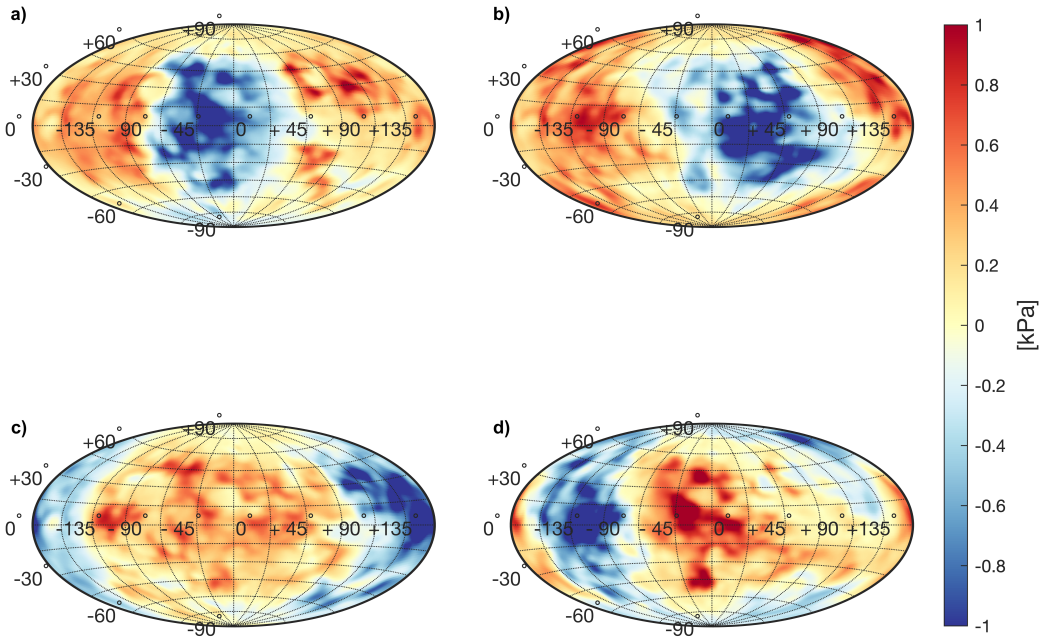

Figure 1 *— Atmospheric pressure anomalies sampled over a Venus solar day. The subsolar point is at 0, 90, 180, 270 degrees in longitude for quadrants a, b, c, d, respectively.*

The GCM model has been evaluated with a sampling of 1 Venus hour (*i.e.*, 24 total samples over 116.752 Earth days) in a 1x1 degree grid. We define the pressure anomaly ΔP as:

$$\Delta P(t,\vartheta,\varphi) = P(t,\vartheta,\varphi) - \langle P(t,\vartheta,\varphi)\rangle \qquad (1)$$

where P denotes the pressure field, t, ϑ,φ the time, latitude, and longitude, respectively, and $\langle\cdot\rangle$ is the time average operator. Figure 1 shows the pressure

anomaly field at local solar times (LST) of 12h, 18h, 24h, and 6h at the prime meridian (0 degree longitude). The pressure anomaly field shows peaks on the order of $1\,kPa$, corresponding to $\sim 103\,ppm$ of the average surface pressure of Venus (96 atm). For a convenient comparison with the static gravitational potential, it is useful to represent the pressure anomaly field in a spherical harmonics series expansion. We use the standard spherical harmonics 4π normalization (*e.g.*, Kaula, 1966), defined by the inner product (over the unitary sphere Ω) between two spherical harmonics base functions Y_{lm} of degree l and order m such that:

$$\int Y_{lm} Y_{l'm'} d\Omega = 4\pi \delta_{ll'} \delta_{mm'} \qquad (2)$$

where δ_{ij} denotes the Kronecker delta operator.

Using this procedure, we can obtain the Stokes coefficients of the spherical harmonics representation of the pressure anomaly ΔC_{lm}^{atm} and ΔS_{lm}^{atm} for each time sample, and thus build a time series of the variation of each individual coefficient.

The transformation from atmospheric pressure anomaly to its gravitational potential counterpart is obtained through Wahr et al. (1998) (the interested reader may refer to Petricca et al. (2022) for a thorough discussion of the topic):

$$\Delta C_{lm}(t) = \frac{3(1+k_l')}{(2l+1)R\rho g_0} \Delta C_{lm}^{atm}(t) \qquad (3a)$$

$$\Delta S_{lm}(t) = \frac{3(1+k_l')}{(2l+1)R\rho g_0} \Delta S_{lm}^{atm}(t) \qquad (3b)$$

where R, ρ, g_0 are the planetary radius, mean density, and surface gravity acceleration, respectively. k_l' are called the loading Love numbers of degree l. Similarly to tidal Love numbers (k_l) these are non-dimensional coefficients relating the forcing potential and the planet's response (Love, 1911). While the tidal Love numbers relate a perturbing gravitational potential (forcing) to the modification of the gravitational potential of the perturbed body (response), the loading Love numbers relate the application of a gravitational normal load to the induced modification of the perturbed body gravitational potential. It is clear then, from Equations 3a and 3b, that

the atmosphere-induced gravitational perturbation can be seen as acting in two different ways. We can identify a *direct* effect, due to the redistribution of atmospheric masses (the 1 in the $(1+k_l')$ term in equations 3a and 3b), and an *indirect* effect, due to the response of the planetary body to the normal loading (k_l' in the $(1+k_l')$ term in equations 3a and 3b). To assess the magnitude of the gravity anomaly induced by the atmospheric mass redistribution it is convenient to compute the amplitude spectrum of the time variable atmospheric anomalies gravity field (C_l in Equation 2.39 of Bertotti et al., 2003). Being a periodic phenomenon, as pointed out by Bills et al. (2020), the spectrum of the atmospheric anomaly gravity field is time-invariant; indeed, it will convey the same information regardless of the time stamp chosen for its computation. Figure 2 reports the comparison between the amplitude spectrum of Venus' static gravity field, as measured by Magellan (MGN180U; Konopliv et al., 1999) and its associated uncertainty, the uncertainty attainable by VERITAS (as simulated by Mazarico et al., 2019) and the computed spectrum of gravity anomalies induced by atmospheric mass redistribution.

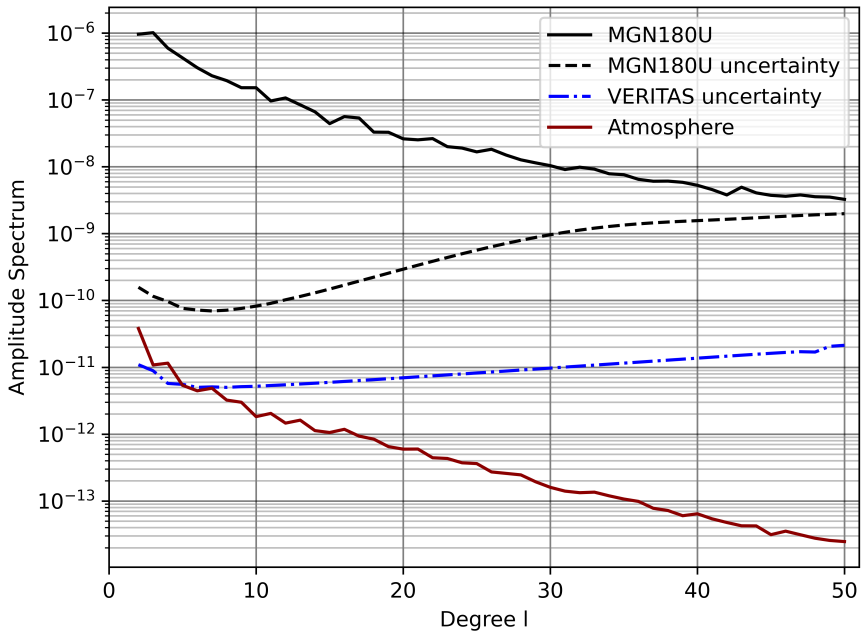

Figure 2 – Comparison between the solid body static gravity field and the atmosphere-induced one. The black solid and dashed lines represent the field and associated uncertainties measured by Magellan, the blue dash-dotted line represent the uncertainty attainable by VERITAS, the red line represents the

amplitude spectrum of the gravity anomalies due to atmospheric mass redistribution. To highlight the low-degree features of the atmospheric gravity field we limit the figure to degree 50.

Figure 2 clearly shows that the gravitational signal of the atmosphere was beyond Magellan's reach but will be above the noise floor attainable by VERITAS. This fact justifies the efforts in studying this phenomenon and assessing whether the atmospheric signal, if not properly modeled, would not bias the gravity science experiment results. It must be noted, however, that the comparison between spectra is not an exact measure of what will be effectively measurable. While it is generally true that a phenomenon having an amplitude spectrum orders of magnitude above the uncertainty will surely be detectable, this approach cannot be used for definitive quantitative estimates in more subtle cases like the VERITAS one, thus justifying and motivating the need of detailed numerical simulations. In previous work (Cascioli et al., 2021) it has been shown that VERITAS will be sensitive to the atmospheric signal and that with proper data analysis strategies, the errors due to an imperfect knowledge of the atmospheric dynamics can be absorbed in the data reduction process without impacting the objectives of the gravity science experiment. More interestingly, given that the expected gravitational signal is higher than the measurement noise floor of VERITAS, it could be possible to probe the main dynamical processes generating it. Equations 3a and 3b show the strong dependency of the gravitational signal to the loading Love numbers which, in turn, depend on the interior structure of the planet (see Section 3). Measured loading Love numbers, in combination with the measurement of the tidal Love number k_2 (real and imaginary parts) and the moment of inertia factor (MOIF), could then impose new and tighter constraints on the interior knowledge.

3. Relation between Love numbers and Venus' interior structure

To determine theoretical values for both Venus' loading Love numbers and its tidal Love numbers, we must first find a solution to the viscoelastic-gravitational problem within the planet (Takeuchi & Saito, 1972). This method has been employed in the study of icy moons (Tobie et al., 2005; Beuthe 2015), Mercury (Goossens et al., 2022; Mazarico et al., 2014), Earth (Martens, 2016), and exoplanets (Bolmont et al., 2020). It assumes spherical symmetry (parameters, such as density, may only vary with radius) and can describe self-gravitating deformations from a variety of sources (tides, surface loading, quakes, or centrifugal flattening). Both the equations of motion and Poisson's

equations can be cast into a set of 4 (for liquid layers; see Equations 11–14 of Kamata et al., 2015) or 6 (for solid layers; see Equations 4–9 of Kamata et al., 2015) ordinary differential equations which are solved as a system starting from the center of the planet. It is common practice to introduce radial functions, y_i ($i \in [1,6]$), to perform these calculations. y_1 and y_3 are associated with the radial and tangential displacements respectively, while y_2 and y_4 are used to find the radial stresses. The total gravitational potential inside the planet is provided by scaling the surface-applied potential by y_5. Finally, y_6 is defined to assist in the application of the surface boundary conditions while maintaining a continuous gravitational potential. The Love numbers are found using the following relationships on these functions calculated for either the tidal or loading surface conditions (*e.g.*, Beuthe, 2015),

$$h = g y_1(R) \quad (4a)$$

$$l = g y_3(R) \quad (4b)$$

$$k = y_5(R) - 1 \quad (4c)$$

where g is the acceleration due to gravity at the surface, and h, l, and k are the radial, tangential, and gravitational Love numbers, respectively (Love, 1911). For a viscoelastic planet, the radial y_i functions are complex-valued; their imaginary parts exist due to the dissipation of energy via frictional heating during tidal or surface loading (see Bagheri et al., 2022, and references therein). These imaginary parts are passed along to the Love numbers and can be used as additional observational constraints if the *phase* (*i.e.*, the angular representation of its complex part) of a given Love number can be measured with reasonable precision (*e.g.*, Dumoulin et al., 2017; Cascioli et al., 2021).

3.1 Solving the Viscoelastic-Gravitational Problem

Several methods have been developed to find the solutions for y_i within a planet, such as the propagator matrix method (*e.g.*, Jara-Orué & Vermeersen, 2011; Sabadini & Vermeersen, 2004) and the shooting method (*e.g.*, Bolmont et al., 2020; Tobie et al., 2005). We choose to use the latter approach as it readily allows for the effects due to compressibility (determined by a finite bulk modulus) to be explored in a computationally stable way (*e.g.*, Beuthe, 2015; Martens, 2015; Bolmont et al., 2021). We have found compressibility to be an important consideration for a planet like Venus, especially for the calculation of loading Love numbers. For example, Figure 3 shows the tidal versus loading

Love number k_2' calculated for the suite of interior models explored in this work (described in Section 3.2) under both the compressible and incompressible assumptions. Previous studies such as Petricca et al. (2022) did not consider the effect of compressibility. By considering compressibility, we observed on average a ~4% larger tidal Love numbers and a ~23% lower loading Love numbers. These differences are larger than the expected measurement uncertainty we calculate in Section 4 (see also Table 3).

Performing the Love number calculations using the shooting method requires first finding a set of solutions to the viscoelastic-gravitational differential equations starting with initial values at the planet's center. These initial values are provided, for example, by Eqs. 100—103 in Takeuchi & Saito (1972) and depend on the local density as well as the shear and bulk moduli of the central core. For solid layers, only three of the solutions are regular at $r = 0$ requiring three different starting solutions. For static[1] liquid layers, there is only one regular solution, and its starting values are provided by Eq. 19 of Saito (1974). Numerical integration of these equations is performed until a phase interface is reached. Interfaces between liquid and solid layers require the multiple solutions to be connected through unknown constants of integration, as well as knowledge about the layer's physical properties, as described in Section 3 of Takeuchi & Saito (1972). These unknown constants are then propagated through the superposition of solutions up to the surface where they are determined by boundary conditions. These boundary conditions vary depending on whether we are calculating the tidal or loading Love numbers (see Table 1).

We performed these numerical integrations using the TidalPy software package (Renaud, 2022) which utilizes a 5th order Runge-Kutta ordinary differential equation integrator with adaptive step sizing.

Table 1: Surface boundary conditions used to calculate both the tidal and loading Love numbers (Beuthe, 2015). In addition to the planet's mean radius, R, and the planet's bulk density, ρ_{bulk}, the Love numbers also depend on the harmonic degree, l, which in the context of tidal dissipation and surface loading is a positive valued integer greater than 0.

[1] In the context of viscoelastic-gravitational solutions, static and dynamic tides refer to an additional dependence on the forcing frequency in the set of differential equations. The static assumption drops this dependence in favor of increased numerical stability (Beuthe, 2015). We will assume the static assumption applies to Venus' thermal tide given its relatively small forcing frequency but note that dynamic tides do play an important role for worlds on short-period orbits as discussed by Kamata et al. (2015).

	Tidal Love Numbers	Loading Love Numbers
$y_2(R)$	0	$-\frac{2l+1}{3}\rho_{bulk}$
$y_4(R)$	0	0
$y_6(R)$	$\frac{2l+1}{R}$	$\frac{2l+1}{R}$

3.2 Interior Structure of Venus

Before these calculations can be made, we must first define the interior structure and physical properties of Venus including the density and shear and bulk moduli as a function of radius. In the case of a viscoelastic planet, the moduli may take the form of complex numbers. In this work we focus on the effects of shear dissipation and assume that the bulk modulus is purely real valued[2]. To calculate the complex shear modulus, we utilize the Andrade rheology (Andrade, 1910; Castillo-Rogez et al., 2011; Renaud & Henning, 2018) which relates the complex shear modulus $\tilde{\mu}$ to the static shear μ, viscosity η, forcing frequency ω, and material properties,

$$\frac{1}{\tilde{\mu}} = \frac{1}{\mu} - \frac{i}{\eta\omega} + \frac{(i\eta\zeta\omega/\mu)^{-\alpha}}{\mu}\Gamma(\alpha+1) \quad (5)$$

where i is the imaginary number and Γ is the Gamma function. The forcing frequency, in the case of surface loading, will largely be driven by atmospheric changes occurring at a period of 116.752 Earth days. Additional material properties of a planet's bulk are parameterized in the Andrade rheology via two dimensionless variables α and ζ (Efroimsky, 2012). α describes, in part, the slope of the shear response versus forcing frequency and viscosity, while ζ is the ratio between the characteristic timescales of anelastic and viscoelastic creep (Renaud & Henning, 2018). Much more experimental work is required to better understand these parameters and any additional dependencies they may share. However, for silicate materials that

[2] The effects of bulk dissipation have been shown to affect tidal heating in the context of rocky moons with significant portion of melt (Kervazo et al., 2021). Its effects on the loading Love numbers will be a topic of future study.

we expect the bulk of Venus' interior to be comprised of, studies have found α and ζ to range between 0.2-0.6 and 0.1-10, respectively. We use the values of $\alpha = 0.3$ and $\zeta = 1$ for our calculations which represent reasonable mid-points in the experimental literature (see Renaud (2019) and the references therein for a review). In Section 5.1 we briefly discuss the impact that the Sundberg-Cooper rheology (Sundberg & Cooper, 2010) may have on Venus' response. We point the interested reader to Renaud & Henning (2018) for a detailed description of this model but note that the key difference between it and the Andrade model described by Equation 5 is an additional Debye-like dissipation peak in both frequency and viscosity space.

Either rheology requires Venus' mantle and core viscosity and shear modulus as inputs, but these properties are presently unknown. Prior work has attempted to model these by performing extrapolations from the Preliminary Earth Reference Model (PREM; Dziewonski & Anderson, 1981; Aitta, 2012) as well as utilizing equations of state on the anticipated interior composition and thermal state of Venus. In this work, we utilize the interior profiles produced by Xiao et al. (2021; hereafter X21) , who considered many different interior configurations including the presence or lack of a solid inner core, and the data produced by Dumoulin et al. (2017; from now on D17; the data was provided by the authors, see Acknowledgment) assuming a purely liquid core. X21 explored twelve major variations on Venus' interior based on whether a solid inner core was present, a cold versus hot mantle (the main difference being the presence of a thick Basalt layer in the mantle for the cold case, see O'Rourke et al. (2018)), and three different parameters used to calculate the mantle viscosity. Each model then had 100 (solid inner core) or 300 (purely liquid core) simulations, where each simulation explored variations in the core-mantle boundary (CMB) temperature (3200—4600 K), the thermal boundary layer thickness (10—200 km), the mantle transition layer thickness (solid inner core only; 10—200 km), the core's sulfur (0—11.8 wt%) and silicon content (0 to 1-χ_{Fe12S}), and the CMB radius (3047—3310 km). D17 also explored a hot and cold mantle for Venus as well as differences in internal composition (see Tables 1 and 2 in D17) and CMB radius (2941—3425 km). We utilize six cases explored by D17, all of which consider a purely liquid core. Unlike X21, D17 does not prescribe a mantle viscosity for their simulations. For these models, we instead use a viscosity that is constant throughout the mantle and rerun the Love number calculations with a different constant viscosity chosen from the range $10^{18} - 10^{22}$ Pa s. As with D17 and X21, we do not consider the case that Venus' core is entirely solid in this work.

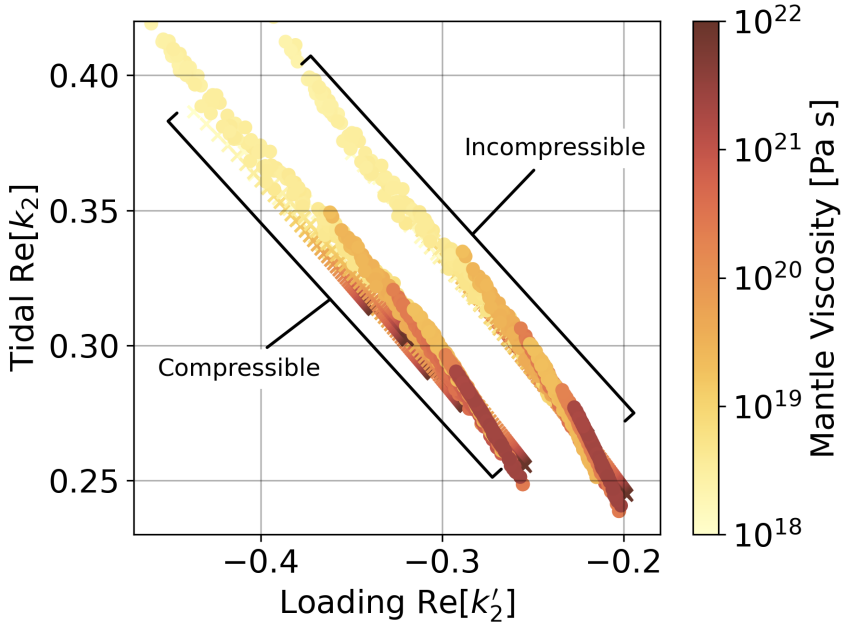

Figure 3 - *Tidal k_2 versus loading k_2' calculated using both the X21 (circles) and D17 (crosses) simulated interiors of Venus. Mantle viscosity is shown as the scatter plot colors. Calculations were performed using the incompressible limit, $K \to \infty$ (right data points) as well as allowing for compressibility and a finite bulk modulus (left data points).*

3.3 Loading Love numbers of Venus

Using the methods described in Section 3.1, we calculate Venus' tidal (see Figures 4a–4d) and loading Love numbers (see Figures 4e–4f) for harmonic degrees $l = 2$ to $l = 10$. In this section we differentiate by models which do and do not contain a solid inner core, as the analysis of observed Love numbers, along with moment of inertia measurements, may help to constrain whether an inner core is present in modern Venus (in analogy to what has been done for Mars, *e.g.*, Rivoldini et al., (2011)). To perform a comparison between these core models, we choose to only show the simulations conducted by X21 and do not analyze the data from D17 which does not consider a solid inner core. This choice was also made as the X21 simulations use a self-consistent viscosity profile for the mantle (see Xiao et al., 2021 Eq. 3), rather than the constant and prescribed values used for D17. This allows us to look at the statistics of multiple simulation runs which range over various model inputs as described in Section 3.2. The average and spread of the 600 X21 simulations (for both a purely liquid and a solid inner core with varying size) are shown in Table 2.

We find that the Love numbers, particularly at low harmonic degree, show moderate variations. We define the relative spread as the separation from the 5^{th} to the 95^{th} percentile of all the model values divided by the average value. The relative spread of k_2 for the liquid core models is over 34% (with a range of 0.272 to 0.376). This spread decreases slightly when a solid inner core is considered with a relative spread of 22.5% and a range of 0.256 to 0.319. The loading Love number k_2' is found to range between -0.410 to -0.276 (average value of -0.313 and relative spread of 43.1%) for a purely liquid core and between -0.325 to -0.262 (average value of -0.286 and relative variation of 22.1%) for a solid inner core. Petricca et al. (2022) found that, for a liquid core, the loading Love numbers ranged between -0.340 to -0.210. Our lower ranges are consistent with the compressibility correction discussed in Section 3.1. Other differences, such as the larger spread in values, arise from our use of the X21 data compared to the use of D17 simulations in Petricca et al. (2022).

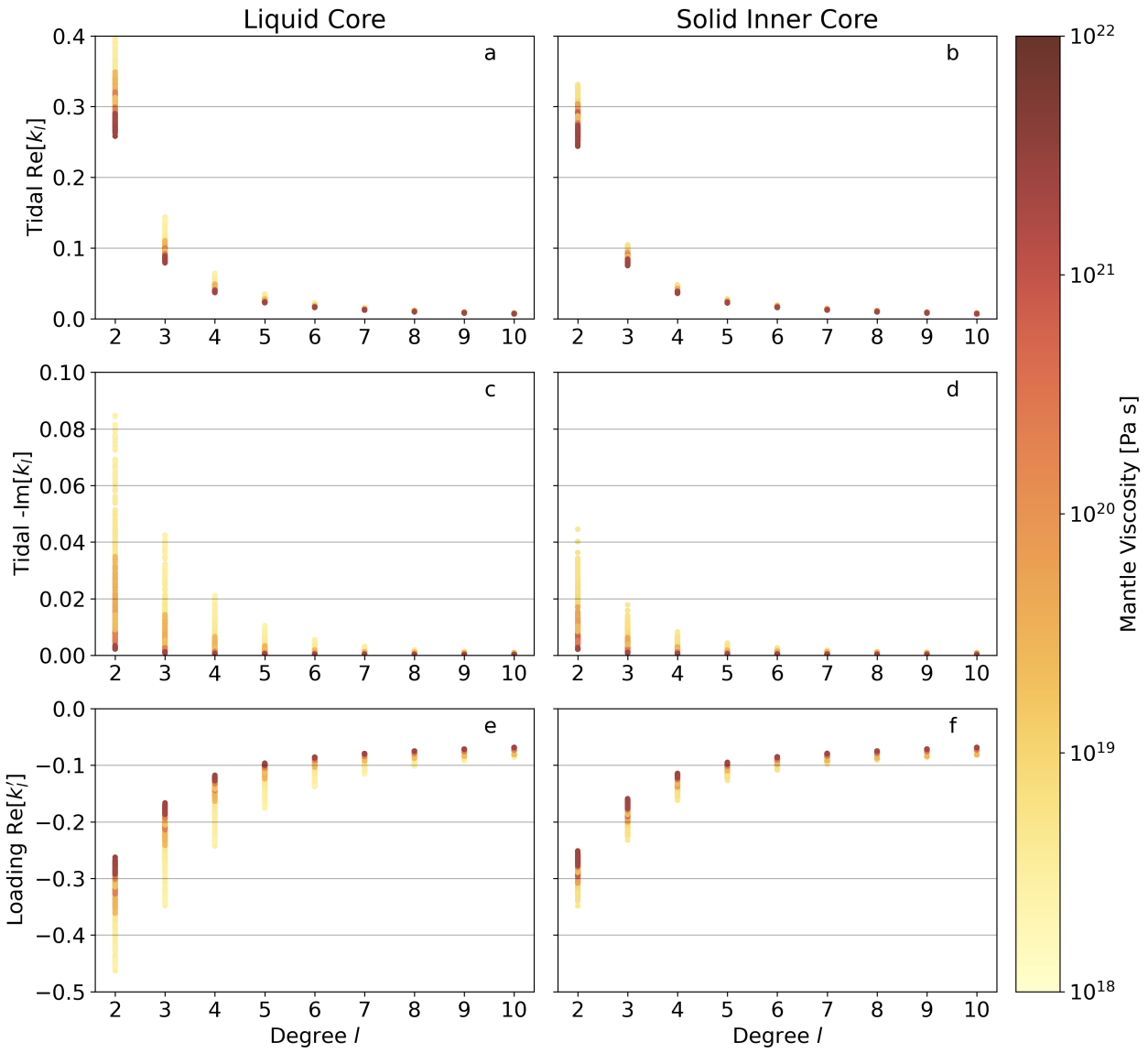

Figure 4: The tidal and loading Love numbers are calculated for harmonic degrees $l = 2$ to $l = 10$ for the purely liquid core models of X21 (left subplots) and those that include a solid inner core (right subplots). We separate out the real portion of the tidal response (subplots a & b), the imaginary portion (subplots c & d), and the real portion of the loading (subplots e & f). Mantle viscosity is shown as the scatter point color.

We confirm the findings of Petricca et al. (2022) that a lower mantle viscosity leads to lower loading Love numbers. The large spread in the values of the imaginary portion of the tidal Love number (200-390% relative spread; see Table 2) suggests a precise measurement of its value may go a long way to constrain the mantle viscosity, with less degeneracy than the real portion alone would provide. We also find that the loading Love number has a semi-asymptotic

relationship with harmonic degree. Converging near -0.08 at high l with only a slight positive slope (see Figures 4e and 4f). These high degrees are thus not sensitive to and diagnostic of the interior structure.

Table 2: The average value and overall spread of the tidal k_l and loading k_l' Love numbers are based on calculations performed on the X21 simulation results for both a purely liquid core and solid inner core models. The ranges are estimated by using the 5-th and 95-th percentile of simulation results, such that 90% of the findings lie within the provided ranges. The percentages were calculated as the difference between those percentiles divided by the average value, to give a sense of the relative spread in values.

		Tidal				**Loading**	
		$\mathrm{Re}[k_l]$		$-\mathrm{Im}[k_l]$		$\mathrm{Re}[k_l']$	
Purely Liquid Core	$l=2$	$0.3045^{+0.0719}_{-0.0324}$	34.3%	$0.0182^{+0.0504}_{-0.0157}$	362%	$-0.3129^{+0.0373}_{-0.0973}$	43.1%
	$l=3$	$0.0950^{+0.0268}_{-0.0115}$	40.3%	$0.0076^{+0.0023}_{-0.0066}$	395%	$-0.2051^{+0.0297}_{-0.0816}$	54.3%
	$l=4$	$0.0434^{+0.0117}_{-0.0049}$	38.1%	$0.0037^{+0.0108}_{-0.0031}$	378%	$-0.1420^{+0.0199}_{-0.0556}$	53.2%
	$l=5$	$0.0258^{+0.0057}_{-0.0025}$	31.9%	$0.0020^{+0.0051}_{-0.0016}$	333%	$-0.1120^{+0.0139}_{-0.0368}$	45.2%
Solid Inner Core	$l=2$	$0.2805^{+0.0385}_{-0.0246}$	22.5%	$0.0095^{+0.0172}_{-0.0072}$	256%	$-0.2857^{+0.0240}_{-0.0390}$	22.1%
	$l=3$	$0.0869^{+0.0133}_{-0.0081}$	24.6%	$0.0036^{+0.0066}_{-0.0027}$	259%	$-0.1839^{+0.0179}_{-0.0302}$	26.2%
	$l=4$	$0.0404^{+0.0055}_{-0.0033}$	21.8%	$0.0019^{+0.0031}_{-0.0014}$	234%	$-0.1294^{+0.0116}_{-0.0205}$	24.8%
	$l=5$	$0.0246^{+0.0028}_{-0.0017}$	18.5%	$0.0012^{+0.0017}_{-0.0008}$	202%	$-0.1049^{+0.0086}_{-0.0144}$	21.9%

4. Sensitivity of radiometric data to loading Love numbers

To quantify the sensitivity of the VERITAS radiometric measurements to the loading Love numbers we have run an extensive set of numerical simulations of the VERITAS gravity experiment aiming to both assess the sensitivity of the tracking system and the robustness of the solution to possible uncertainties in the mismodeling of the atmospheric pressure field. The gravity science experiment is based on the collection of two-way coherent X- and Ka-band radiometric measurements. The radio tracking system of VERITAS has heritage from ESA's BepiColombo and will obtain an end-to-end accuracy ranging between 0.015 and 0.038 mm/s at 10-s integration time (Cappuccio et al., 2020; Iess et al., 2021). In this work we have implemented a noise model which accounts for all the main noise sources (solar plasma, Earth troposphere, ground station frequency stability, antenna mechanical noise,

etc.) reflecting the latest results of BepiColombo. The model has been tuned to reflect the VERITAS requirement of an end-to-end noise of 0.033 mm/s over 10-second integration times outside of solar conjunctions (Sun-Venus-Earth angle > 15 degrees). VERITAS will also collect radar tie points (repeated observations of the same surface feature) from the interferometric synthetic aperture radar VISAR (Hensley et al., 2020). The radar tie points will greatly contribute to the scientific return of the mission by strongly tying the motion of the probe to the rotational state of the planet, thus significantly increasing the sensitivity of the experiment to the planet's moment of inertia (Cascioli et al., 2021). The expected noise level for radar tie points is 10 HZ and 3m for their Doppler and range components, respectively (See Cascioli et al., 2021 Appendix 1 for additional details). The numerical simulation setup, based on NASA-JPL MONTE (Evans et al., 2018) is identical to the one used in our previous works. We summarize here the main features: the orbit determination (OD) problem is formulated in its multi-arc form (Milani & Gronchi, 2009) meaning that the solved-for parameters are divided in two groups: local and global. The local parameters are the ones influencing a single data arc ~~(here chosen to last three days)~~ while the global parameters have influence over the whole mission (*e.g.*, the Venus gravity field). We subdivide the nominal mission time span (~4 Venus sidereal days corresponding to ~2.7 years) into 324 arcs lasting 3 days each. We estimate, besides the atmospheric gravity field-related parameters discussed in the next section, the gravity field of Venus up to degree and order 50 (as higher degrees do not affect the estimate of long characteristic-time phenomena like the ones we are interested in here), the tidal Love number k_2 (both real and imaginary), the planetary body-fixed spin axis orientation and orientation-rate (precession). We also estimate the sidereal period as a local parameter, to account for possible short-term variability (Margot et al., 2021), a scale factor per arc for the solar radiation pressure and we model (and estimate) the drag coefficient as a stochastic parameter with an update time of 30 minutes. For a more details on the simulation and filter setup, we refer the reader to Cascioli et al. (2021).

4.1 Measuring the loading Love numbers

The core of the gravity science experiment of VERITAS relies on the solution of an OD problem. An OD problem consists in finding the set of parameters of the dynamical model of the spacecraft (the *state* of the problem) which

minimizes the discrepancy between the actual measurements collected by the ground station and radar (observed observables) and the measurements predicted through the said dynamical model (computed observables). In its linear least squares formulation (for a detailed description, see Tapley et al., 2004 or Cascioli & Genova, 2021), the minimum variance estimator of the *state* correction $\hat{x}$ is given by:

$$\hat{x} = (H^T R^{-1} H + \bar{P}^{-1})(H^T R^{-1} y + \bar{P}^{-1}\,\bar{x}) \qquad (6)$$

where R is the covariance matrix of the measurement noise, $\bar{P}$ is the a-priori covariance matrix of the state, $\bar{x}$ is the vector of a-priori values of the state, and y is the vector of observation residuals (the difference between observed and computed observables). H is the so-called mapping matrix, which collects the partial derivatives of the observations with respect to the state. To include the estimation of the loading Love numbers in the OD filter, a suitable mathematical representation of the gravitational anomalies due to the atmosphere must be developed.

Leveraging the periodic nature of the atmospheric thermal tides, the time series of the pressure anomaly Stokes coefficients $\Delta C_{lm}^{atm}(t)$ and $\Delta S_{lm}^{atm}(t)$ can be expanded in Fourier series:

$$\Delta C_{lm}^{atm}(t) = \sum_f A_{lm}^C cos(2\pi f t) + B_{lm}^C sin(2\pi f t) \quad (7a)$$

$$\Delta S_{lm}^{atm}(t) = \sum_f A_{lm}^S cos(2\pi f t) + B_{lm}^S sin(2\pi f t) \quad (7b)$$

The summation is performed over harmonics of the forcing period T_s, *i.e.*, at frequencies $f = \frac{1}{T_S}, \frac{2}{T_S}, \ldots, \frac{N}{T_S}$. The Fourier expansion is limited by the number of samples extracted from the time series of pressure grids. The harmonic representation of the gravity anomalies is very convenient for forward modeling the phenomenon, leaving the modeler the ability to easily disentangle and select the different frequency contents of the signal.

Since the same k_l' holds for both $\Delta C_{lm}(t)$ and $\Delta S_{lm}(t)$, Equations 3a and 3b can be summed together:

$$\Delta C_{lm} + \Delta S_{lm} = \frac{3(1+k_l')}{(2l+1)R\rho g_0}\ (\Delta C_{lm}^{atm} + \Delta S_{lm}^{atm}) \quad (8)$$

from which the partial derivative of the measurement y with respect to the loading Love number of degree l is computed applying the chain rule:

$$\frac{\partial y}{\partial k_l'} = \sum_m \frac{\partial y}{\partial \Delta C_{lm}} \frac{\partial \Delta C_{lm}}{\partial k_l'} + \frac{\partial y}{\partial \Delta S_{lm}} \frac{\partial \Delta S_{lm}}{\partial k_l'} \quad (9)$$

where:

$$\frac{\partial \Delta C_{lm}}{\partial k_l'} = \frac{3}{(2l+1)R\rho g_0} \Delta C_{lm}^{atm} \quad (10a)$$

$$\frac{\partial \Delta S_{lm}}{\partial k_l'} = \frac{3}{(2l+1)R\rho g_0} \Delta S_{lm}^{atm} \quad (10b)$$

The terms $\frac{\partial y}{\partial \Delta C_{lm}}$ and $\frac{\partial y}{\partial \Delta S_{lm}}$ can be computed by observing that the instantaneous partial derivative of the observable with respect to ΔC_{lm} and ΔS_{lm} is identical to the partial derivative with respect to static C_{lm} and S_{lm}. The latter are very well known and already implemented in the majority of OD codes (*e.g.*, Moyer 2003).

Equation 9 has to be evaluated at the epoch of each observation, which in general will differ from the time samples of the pressure grids obtained from the GCM. The values of ΔC_{lm}^{atm} and ΔS_{lm}^{atm} in the right-hand side of Equation 10a and 10b are thus computed from their Fourier series expansion.

With this procedure, we add the loading Love numbers up to degree 5 to the OD filter as global parameters. We choose degree 5 as a cutoff after having verified, through preliminary simulations, that higher degrees are not measurable due to a low signal to noise ratio (see also Figure 2). As evidenced by Equations 3a and 3b, the gravity anomalies induced by the atmospheric mass redistribution do not depend on the loading Love numbers alone and are strongly driven by the underlying forcing atmospheric pressure field. Assuming that the uncertainty of the estimated k_l' matches with their formal errors extracted from the OD filter could possibly lead to an underestimation of the propagation of GCM uncertainties. Recent studies show a good match between the structure of the thermal tides predicted by GCMs and the in-situ measurements collected by Venus Express' VIRTIS (Scarica et al., 2019) for altitudes >60 km. However, the amplitude of the uncertainty or error expected in atmospheric pressure anomaly fields at the surface has not been similarly ascertained. For this reason, in our simulations we perturb both the atmospheric pressure field and the static body gravity field. This implies that we use the nominal models to generate the synthetic

observables used as *truth* in the orbit determination procedure and the perturbed models in the retrieval process. In the following we will report both the formal uncertainty and the estimation error (difference between estimate and truth), which more realistically reflects the true attainable uncertainty.

In our simulation, the static gravity field measured by Magellan has been perturbed from its measured covariance (Konopliv et al., 1999). For what pertains to the atmospheric pressure field, we have run different cases to quantify the effect of possible GCM mismodeling. We identified two main ways of perturbing the atmospheric pressure anomaly field: perturbing the pressure grid prior to its expansion into spherical harmonics and Fourier series, and perturbing directly the Fourier series coefficients. Comparisons between GCM predictions and in-situ observations have shown thermal anomalies differences in the order of 5-10 K at ~60 km altitude (Scarica et al., 2019). These differences map into relative variations of the pressure anomalies in the order of 1%. Because of the very different mechanisms regulating the surface pressure and the cloud region (~60 km), a direct extrapolation of these comparison studies cannot be adopted. Thus, we have chosen a conservative approach and adopt perturbations of 10% on the pressure anomaly grids for our simulations.

Because of their different nature, the two perturbation methods lead to different magnitude of the resulting perturbed gravity anomalies. To obtain the same effect of perturbing the pressure grid at the 10% level, the Fourier coefficients need to be perturbed at the 2% level. Figure 5 shows the relative difference in the gravity anomalies using both perturbation methods. It is interesting to highlight the difference between the two methods: directly perturbing the pressure grid (Figure 5, top panel) consists in applying a near-white noise over the whole grid, thus locally perturbing the atmospheric value while maintaining the underlying pressure anomaly geospatial structure. On the other hand, perturbing the Fourier expansion coefficients results in a modification of the spatio-temporal structure of the pressure anomaly field, which may better mimic mismodeling of the physical processes embedded in the GCM models.

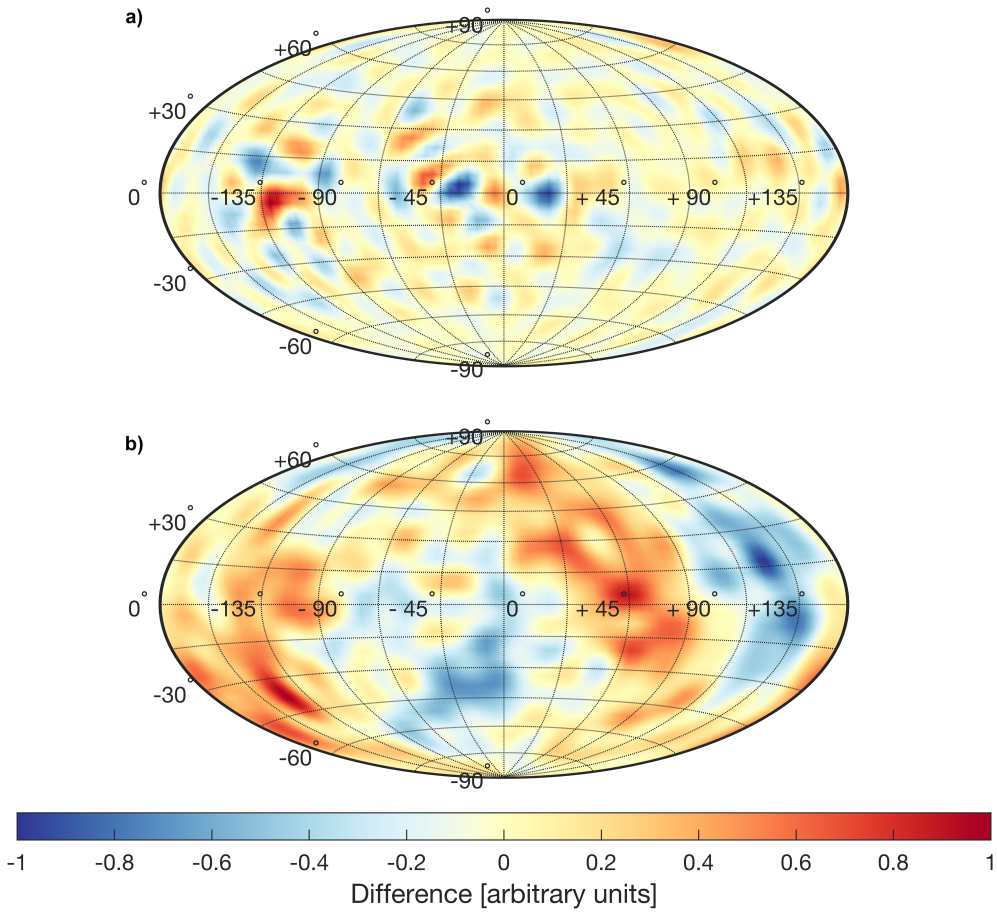

Figure 5: Gravity anomalies due to pressure field perturbations. The color scale represents differences between the perturbed and unperturbed fields rescaled between -1 and 1. (a) shows the gravity anomalies differences when perturbing the pressure anomaly grid, (b) shows the gravity anomalies differences when perturbing the Fourier series expansion coefficients.

4.2 Results

We run the numerical simulations for the two distinct perturbation cases discussed in the previous paragraph. From now on we will refer to the pressure grid perturbation as Solution P (SOL-P) and the Fourier coefficients perturbation as Solution F (SOL-F). We first simulate the gravity experiment using Doppler tracking only (no radar tie points) to prove the capability of measuring the loading Love numbers with Doppler data alone. A discussion of the attainable results when performing a combined Doppler-tie points analysis will follow shortly after.

We have run a full recovery study (not a covariance analysis) to probe the systematic errors introduced after perturbing the atmospheric input and other

parameters such as the loading Love numbers and the static gravity field coefficients. In a covariance simulation, only the formal estimation uncertainty of the parameters is recovered; in a full simulation, all the parameters are initially perturbed, and thus the estimation errors are also obtained, which account for the effect of systematic effects and correlations. Table 3 reports the simulation results in terms of formal uncertainty and estimation error on the parameters of interest. The orbit determination solution shows to be robust to this magnitude of atmospheric perturbation, as testified by a general good quality of the fit. We find that the estimation errors are comparable with the formal uncertainties. As expected, the radiometric observables are mainly sensitive to the degree-2 loading Love number k_2' whose expected error, which we choose as the maximum between the formal uncertainty and estimation error for SOL-P and SOL-F, corresponds to a 9.7% spread compared to the k_2' range (5^{th}-95^{th} percentile) predicted by the various interior models we tested (see Table 2). The degrees 3 and 4 are less strongly recovered, while k_5' is not resolved as its uncertainty is larger than the modeled range (> 100%). These results suggest that the measurement of k_2' (and more marginally k_3' and k_4') could help in discriminating between plausible interior structure models.

As discussed in previous work (Cascioli et al., 2021) the combined analysis of Doppler tracking and radar tie points can substantially augment the sensitivity to the rotational state of the planet, leading to nearly an order of magnitude reduction of the uncertainty on the moment of inertia factor (MOIF). The inclusion of tie points in the analysis has the beneficial effect of strengthening the trajectory reconstruction of the probe through a better determination of the parameters related to non-gravitational forces in the filter, particularly by bringing new measurements outside of the radio tracking periods (Cascioli et al., 2022). This process has been proven to benefit the retrieval of the Love numbers as well, with a factor 2-3 reduction in the uncertainties of the tidal Love number and the associated tidal lag. Having demonstrated that the OD filter can consistently recover perturbations in the atmospheric model, we report in Table 3 the results of a covariance simulation using the combination of Doppler and tie points (because of the dramatic increase in computational expense of a full perturbed inversion when using tie points, we only performed a covariance simulation, with resulting formal uncertainty values but no derived biasing errors). The inclusion of tie points enables a reduction of the uncertainty of k_2' by a factor of ~2.5, in line with the improvement on the tidal Love number of degree 2 (see Table 1 in Cascioli et al., 2021). The reduction in uncertainty

is particularly significant for k_4' which, under these assumptions, can be now determined at the 17% level. From these results, we can conclude that VERITAS will be able to reliably measure k_2' in a Doppler-only configuration but also k_3' and k_4' using the combined analysis of Doppler and radar tie points.

Table 3: Formal uncertainties and estimation errors on the main parameters of interest in the two simulated Doppler only cases (SOL-P and SOL-F) and formal uncertainties in the Doppler + tie points case. We also report the expected uncertainty (the max between formal uncertainty and estimation error A and B) as a percentage of the maximum expected variability of the loading Love numbers (defined as the width of the 5th-95th percentiles, discussed in Section 5).

	Doppler only				Doppler + Tie Points	
		Solution P	Solution F			
Parameter	Formal Uncertainty	Estimation Error	Estimation Error	Percentage of max. variability	Formal uncertainty	Percentage of max. variability
$Re[k_2]$	4.0×10^{-4}	5.3×10^{-4}	7.1×10^{-4}	-	1.2×10^{-4}	-
$Im[k_2]$	3.9×10^{-4}	4.6×10^{-4}	3.9×10^{-4}	-	1.2×10^{-4}	-
$MOIF$	4.3×10^{-3}	9.0×10^{-4}	8.5×10^{-4}	-	5.0×10^{-4}	-
k_2'	1.3×10^{-2}	8.0×10^{-3}	6.3×10^{-3}	9.7%	5.0×10^{-3}	3.7%
k_3'	5.0×10^{-2}	4.2×10^{-2}	4.8×10^{-2}	45%	4.0×10^{-2}	35%
k_4'	3.2×10^{-2}	2.0×10^{-3}	4.7×10^{-2}	62%	1.3×10^{-2}	17%
k_5'	6.8×10^{-2}	8.8×10^{-2}	9.6×10^{-3}	170%	4.0×10^{-2}	79%

5. Interior structure and rheological constraints arising from VERITAS measurements

The observational constraints described in Section 4 will define a 3-dimensional measurement in the phase space of Venus Love numbers, namely the real and imaginary portions of the degree-2 tidal Love number at the tidal forcing period of 58.3 days (frequency ω_T), and the real portion of the loading Love number. Since the diurnal thermal tides are the principal contribution to the atmospheric loading, the loading Love numbers are assumed

to be measured at the solar forcing period of 116.75 days (frequency ω_S). In concert, these three values (along with other measurements of, *e.g.*, the moment of inertia factor, k_3', k_4') can be used to determine the most likely interior and thermal state of Venus in both a structural and rheological context. In Figure 6, we show how measurements made by VERITAS can narrow the most likely mantle viscosity for the planet. The small observational uncertainties (shown as error bars in the figure) calculated in Section 4 for the real and imaginary tidal Love numbers are small enough for future VERITAS measurements to isolate a small number of likely interior models from those considered by X21 and D17. These two parameters cannot alone capture the entire spectrum of possible models since, as shown in Figure 6, this would correspond to projecting the whole model cloud onto the (Re[k_2], Im[k_2]) plane, losing information from the third dimension provided by the loading Love number. The uncertainty in the loading Love number, although substantially larger, can further constrain the likely composition, viscosity, as well as other rheological parameters. As we will discuss in Section 5.1, it provides additional and independent information especially in a low viscosity scenario, where the non-completeness of the Re[k_2], Im[k_2] pair in describing the full model space becomes more evident.

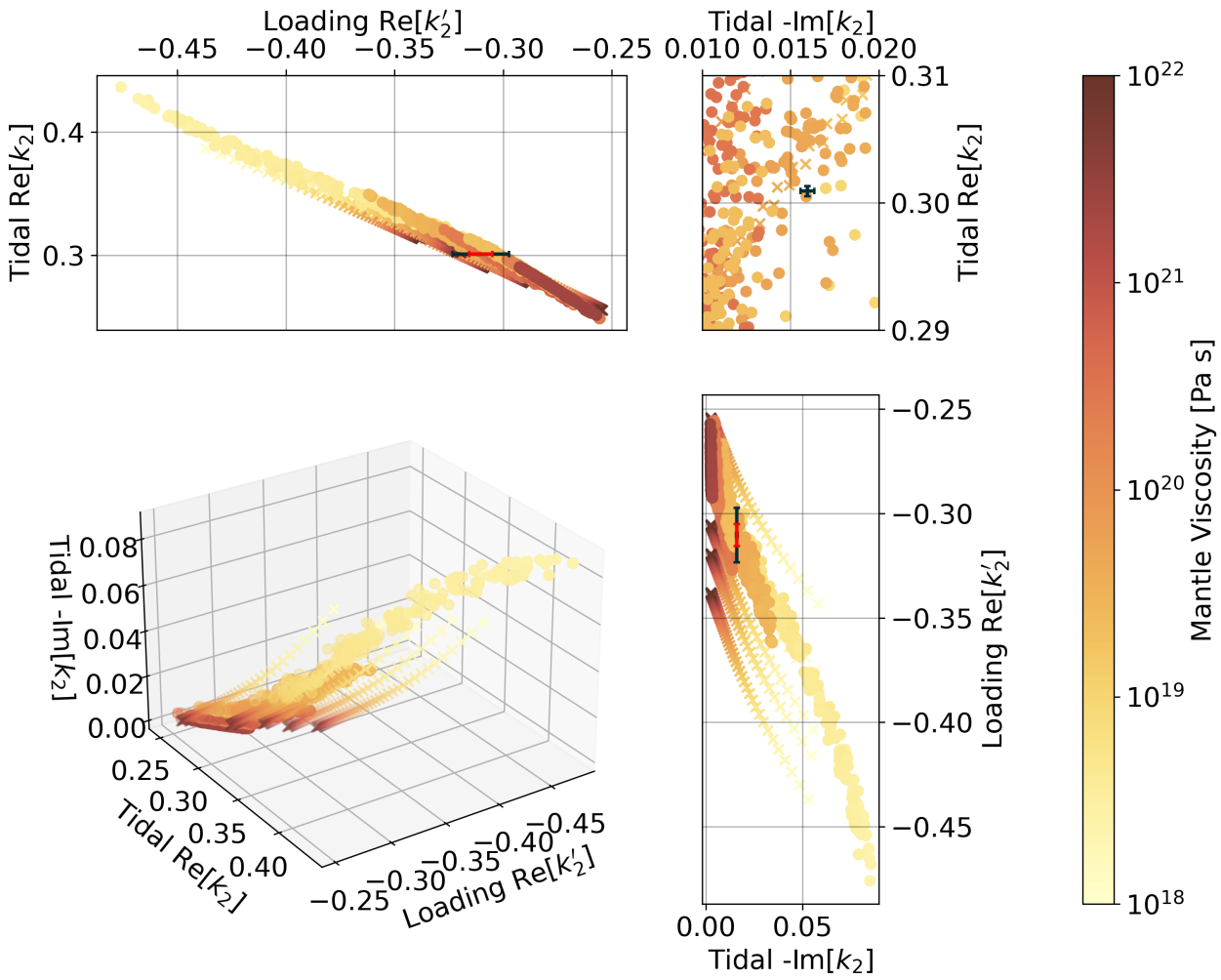

Figure 6: The tidal and loading Love numbers are shown in a 3-dimensional phase space with mantle viscosity shown as the color bar. Error bars are fixed at the average values found for the calculations made using the simulations from both X21 (circles) and D17 (crosses). The lengths of the error bars are taken from the expected VERITAS observational uncertainties calculated in Section 4 (black: Doppler only, red: Doppler + tie points). The upper right panel is zoomed in on the average Re[k_2] and -Im[k_2] to emphasize the small observational error we expect for these measurements and how the observed values can be used to accurately discern from the large number of possible interior states.

In general, we find that higher -Im[k_2], higher Re[k_2], and lower Re[k_2'] correspond to lower mantle viscosities. We also see, in Figure 7, that this configuration suggests a larger core size. The loading Love number is a particularly useful tool in constraining core size which is more degenerate in the tidal Love number space, however the larger observational errors may

prove too large to accurately constrain core size from the loading Love number alone. Future work utilizing a Monte-Carlo Markov Chain examination of various input parameters will be performed to determine, quantitatively, how the addition of the loading Love number can narrow the phase space of possible interior configurations and thermal states. These studies will also help to quantitatively understand if a measurement of the higher degree loading Love numbers (*e.g.*, $l = 3 - 5$) at the level of uncertainty reported in Table 3 can be useful in providing additional constraints in the interior structure inversion process.

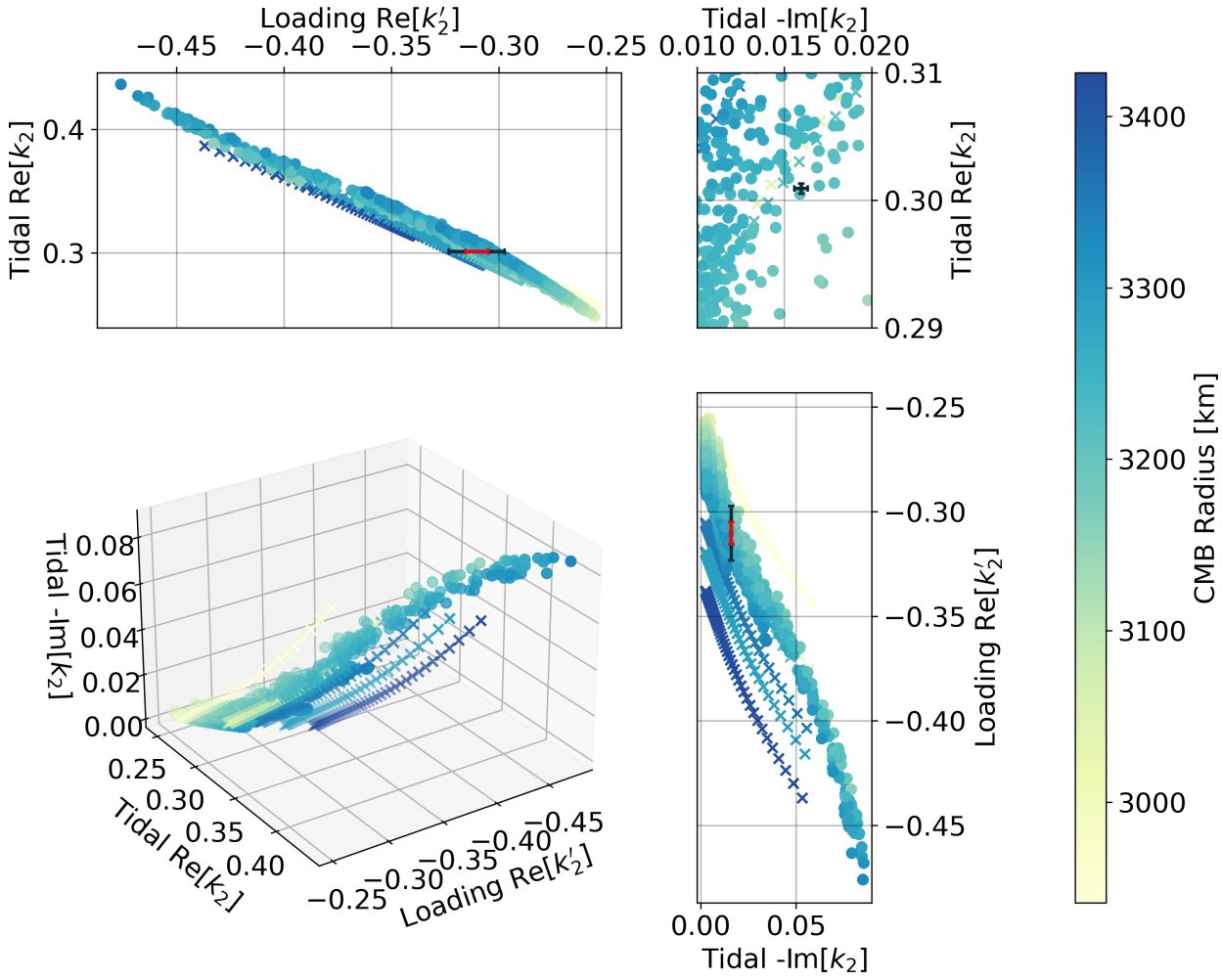

Figure 7: The same phase space that was shown in Figure 6 is repeated here now with core-mantle-boundary radius shown as the color bar.

5.1 Loading Love numbers as a tool for probing the planet response at different forcing frequencies

There exist well-determined relationships between different sets of Love numbers. For example, Saito (1978) gives:

$$k'_l = k_l - h_l \quad (14)$$

where h is the vertical displacement tidal Love number, relating the tidal gravitational perturbation to the radial displacement of the surface of the body (for a given degree l). Petricca et al. (2022) suggested that a combined measurement of k_2 and k'_2 will provide an indirect measurement of h_2. However, this relationship may have limited applicability if the viscosity of the mantle is low, as we will show in the following. When considering the viscoelastic gravitational problem, this relationship is formally correct only at a given forcing frequency ω:

$$k'_l(\omega) = k_l(\omega) - h_l(\omega) \quad (15)$$

At Venus, this means that the loading Love number (measured at the loading frequency ω_S) and the tidal Love numbers (measured at the tidal frequency ω_T) cannot be directly tied via Equation 14, as they are driven at two different forcing periods. We compared k'_2 with $k_2 - h_2$ from our model computations, and the disagreement with Equation 14 is particularly clear for low values of the mantle viscosity, as shown in Figure 8, where the frequency-dependent dissipation plays a major role. Inferring the value of $h_2(\omega_T)$ from the estimates of $k_2(\omega_T)$ and $k'_2(\omega_S)$ using Equation 14, as suggested by Petricca et al. (2022), is not formally correct, although we recognize in practice Equation 14 may appear to hold, if measurement uncertainties are large or if the Venus mantle viscosity is high (>10^{21} Pa s). The deviation of the viscoelastic interior model values from the linearity given by Equation 14, for low viscosity values, makes explicit the importance of an accurate measurement of k'_2 as the full spectrum of possible interior models cannot be described with two parameters (linear relation between real and imaginary Love numbers).

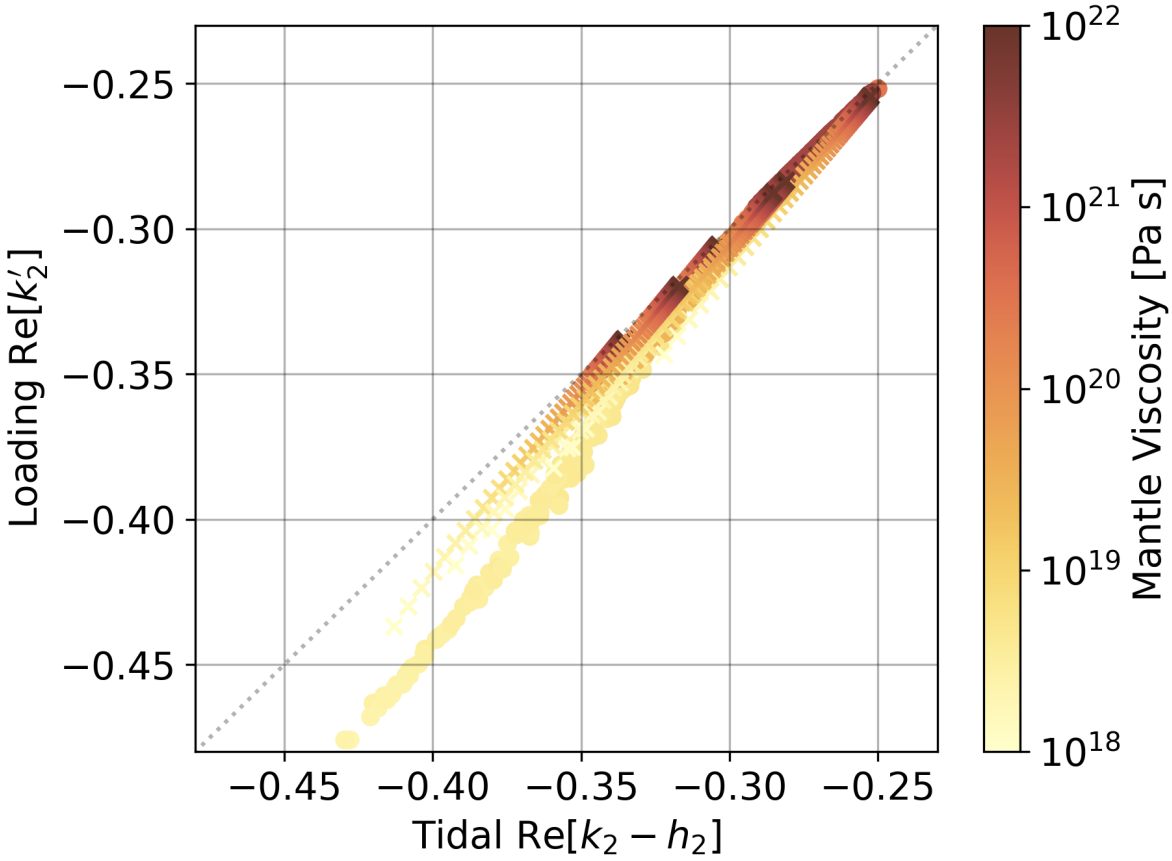

Figure 8: Graphical representation of Equation 15. k_2' is shown versus $k_2 - h_2$. Calculations were performed on the interior models from X21 (circles) and D17 (crosses). The diagonal dotted line represents the theoretical value k_2' obtained from k_2 and h_2 under the assumption of Equation 14.

Until now we have discussed the direct comparison between $k_2(\omega_T)$ and $k_2'(\omega_S)$, however, we will show here that Equation 15 can be exploited to obtain further information on the frequency-dependent response of the planet. Using Equation 15, we can obtain an estimate of the loading Love number at the *tidal* frequency $k_2'(\omega_T)$ from the measurements of $k_2(\omega_T)$ and $h_2(\omega_T)$.

$$k_2'(\omega_T) = k_2(\omega_T) - h_2(\omega_T) \qquad (16)$$

Indeed, we have already discussed the fact that VERITAS will measure the tidal Love number $k_2(\omega_T)$, and it is worth recalling now that thanks to the combined Doppler and radar tie points analysis, VERITAS will be sensitive to the Love number $h_2(\omega_T)$ with an accuracy of 5×10^{-2} (1σ, under very conservative

assumptions; Cascioli et al., 2021). To first approximation, we can assume that $\sigma(k_2'(\omega_T)) \cong \sigma(h_2(\omega_T)) = 5 \times 10^{-2}$ thus resulting in an estimate of $k_2'(\omega_T)$ with an accuracy of ~35% of the expected range[3].

It is important to underline that the measurement of $k_2'(\omega_T)$ is completely model independent, relying only on the very general assumptions needed to obtain Equation 15.

It is also worth highlighting that the $\sigma(h_2(\omega_T))$ reported here has been obtained with very conservative assumptions, both in terms of modeling and for the number of considered radar tie points (<10% of the predicted total number of tie points detectable by the on-board radar). We can plausibly foresee that substantially lower h_2 uncertainties will be attained by VERITAS.

The power of the concurrent measurement of $k_2'(\omega_S)$ and $k_2'(\omega_T)$ is the ability to constrain two points on the amplitude-frequency curve for the loading Love number (see Figure 9). We argue that this may help discriminate different rheological laws, and ascertain parameters governing a given rheology. The precise quantification of the constraining power of these measurements, in combination with other key geophysical parameters estimates (such as the MOIF), would require a full inversion of the interior structure model of Venus (*e.g.*, using Monte Carlo Markov Chain techniques). This task goes beyond the scope of this work, and will be part of future focused follow-on investigations.

[3] We have verified that the expected variation range of $k_2'(\omega_T)$ spans the same range of $k_2'(\omega_S)$

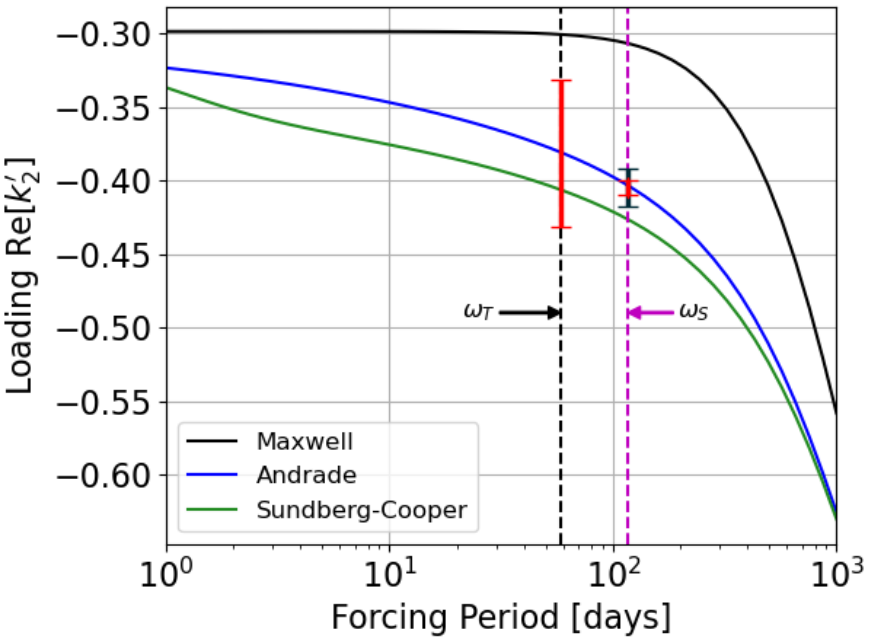

Figure 9: Degree-2 loading Love number amplitudes are shown as a function of the forcing period for three different rheological laws (Maxwell, black line; Andrade, blue line; and Sundberg-Cooper, green line). We report the expected accuracy of the two measurements of the loading Love numbers as the black error bars centered on the Andrade line (the red error bar represents the results expected from the Doppler and tie points combined analysis, while the black error bar represents the Doppler only case). The vertical magenta and black dashed lines represent the loading and tidal forcing frequencies, respectively.

6. Conclusion

In this work we have investigated the capability of the VERITAS gravity science investigation to measure the Venus loading Love number. As demonstrated in previous studies, VERITAS will be sensitive to the thermal tides arising in the Venus atmosphere due to the solar radiative input. The gravitational signal of this phenomenon depends on the interior structure of the planet, through the loading Love numbers, and we have conducted an extensive set of numerical simulations showing that VERITAS will be able to reliably determine the low-degree loading Love numbers. We have compared the predicted measurement uncertainties with the latest models of Venus interior available in literature and shown that a concurrent measurement of the tidal and loading response of the planet could indeed provide useful information to distinguish between different classes of Venus interiors, especially in the case of a low mantle viscosity. We have further described how the frequency dependence of the tidal

response of the planet can be leveraged to probe the rheology (and its defining parameters). In particular, we have shown that the frequency dependence of k_2, k_2' and h_2 can be leveraged to constrain the response of the planet at two different forcing periods, the loading frequency and the tidal frequency, by making use of known relationships between the Love numbers. Important information about the interior of Venus may be obtained by the combination of all these parameters, which the VERITAS mission is uniquely placed to measure in the near future. A more quantitative assessment of the contribution of these measurements in the inversion of the full interior structure of Venus will require a focused follow-on study (*e.g.*, using Monte Carlo Markov Chain estimation techniques).

Acknowledgements

The expansion of the surface pressure grids into spherical harmonics coefficients has been performed with the pyshtools Python library (Wieczorek & Meschede, 2018). Tidal and load number calculations were performed utilizing the TidalPy and CyRK (Renaud, 2022, 2023) software packages. The authors would like to thank Flavio Petricca (Sapienza University) for useful discussions and suggestions. We would like to thank Caroline Dumoulin for providing the data from Dumoulin et al. (2017) which was used in this work, and the authors of Xiao et al. (2021) for publicly releasing the full dataset associated with their manuscript (which can be found in Xiao, 2019). G.C. and J.P.R. would like to acknowledge support for this work from NASA under award number 80GSFC21M0002. G.C. and E.M. acknowledge support from the VERITAS mission. J.P.R. and S.G. acknowledges support from the Planetary Geodesy Internal Scientist Funding Model work package funded by the NASA Planetary Science Division. D.D and L.I. would like to acknowledge support for this work from the Italian Space Agency (ASI) under contract number 2022-15-HH.0.

Data availability

The software used for computing the Love numbers and the values of the computed Love numbers (tidal and loading) for each of the analyzed interior structure models will be available at Zenodo (10.5281/zenodo.7668227) and at the NASA Goddard Planetary Geodynamics Data Archive (PGDA) website (https://pgda.gsfc.nasa.gov/products/89)

Conflict of Interest

The authors declare that they have no conflict of interest.

References

Aitta, A. (2012). Venus' internal structure, temperature and core composition. *Icarus*, *218*(2), 967–974. https://doi.org/10.1016/j.icarus.2012.01.007

Andrade, E. N. D. C. (1910). On the viscous flow in metals, and allied phenomena. *Proceedings of the Royal Society of London. Series A, Containing Papers of a Mathematical and Physical Character*, *84*(567), 1–12. https://doi.org/10.1098/rspa.1910.0050

Bagheri, A., Efroimsky, M., Castillo-Rogez, J., Goossens, S., Plesa, A.-C., Rambaux, N., Rhoden, A., Walterová, M., Khan, A., & Giardini, D. (2022). Tidal insights into rocky and icy bodies: An introduction and overview. In *Advances in Geophysics* (Vol. 63, pp. 231–320). Elsevier. https://doi.org/10.1016/bs.agph.2022.07.004

Bertotti, B., Farinella, P., & Vokrouhlický, D. (2003). *Physics of the Solar System* (Vol. 293). Springer Netherlands. https://doi.org/10.1007/978-94-010-0233-2

Beuthe, M. (2015). Tidal Love numbers of membrane worlds: Europa, Titan, and Co. *Icarus*, *258*, 239–266. https://doi.org/10.1016/j.icarus.2015.06.008

Bills, B. G., Navarro, T., Schubert, G., Ermakov, A., & Górski, K. M. (2020). Gravitational signatures of atmospheric thermal tides on Venus. *Icarus*, *340*, 113568. https://doi.org/10.1016/j.icarus.2019.113568

Bolmont, E., Breton, S. N., Tobie, G., Dumoulin, C., Mathis, S., & Grasset, O. (2020). Solid tidal friction in multi-layer planets: Application to Earth, Venus, a Super Earth and the TRAPPIST-1 planets: Potential approximation of a multi-layer planet as a homogeneous

967 body. *Astronomy & Astrophysics*, *644*, A165. https://doi.org/10.1051/0004-
968 6361/202038204
969 Cappuccio, P., Notaro, V., Ruscio, A. di, Iess, L., Genova, A., Durante, D., Stefano, I. di, Asmar,
970 S. W., Ciarcia, S., & Simone, L. (2020). Report on First Inflight Data of BepiColombo's
971 Mercury Orbiter Radio Science Experiment. *IEEE Transactions on Aerospace and*
972 *Electronic Systems*, *56*(6). https://doi.org/10.1109/TAES.2020.3008577
973 Cascioli, G., Durante, D., Mazarico, E., Wallace, M., Hensley, S., & Smrekar, S. (2022).
974 Improving the VERITAS Orbit Reconstruction Using Radar Tie Points. *Journal of*
975 *Spacecraft and Rockets*, 1–8. https://doi.org/10.2514/1.A35499
976 Cascioli, G., & Genova, A. (2021). Precise Orbit Determination Technique to Refine Spacecraft
977 Mechanical Modeling. *Journal of Spacecraft and Rockets*, *58*(2), 581–588.
978 https://doi.org/10.2514/1.A34922
979 Cascioli, G., Hensley, S., Marchi, F. D., Breuer, D., Durante, D., Racioppa, P., Iess, L.,
980 Mazarico, E., & Smrekar, S. E. (2021). The Determination of the Rotational State and
981 Interior Structure of Venus with VERITAS. *The Planetary Science Journal*, *2*(6), 220.
982 https://doi.org/10.3847/PSJ/ac26c0
983 Castillo-Rogez, J. C., Efroimsky, M., & Lainey, V. (2011). The tidal history of Iapetus: Spin
984 dynamics in the light of a refined dissipation model. *Journal of Geophysical Research*,
985 *116*(E9), E09008. https://doi.org/10.1029/2010JE003664
986 Davaille, A., Smrekar, S. E., & Tomlinson, S. (2017). Experimental and observational evidence
987 for plume-induced subduction on Venus. *Nature Geoscience*, *10*(5), 349–355.
988 https://doi.org/10.1038/ngeo2928

989 Dobrovolskis, A. R., & Ingersoll, A. P. (1980). Atmospheric tides and the rotation of Venus I.
990 Tidal theory and the balance of torques. *Icarus*, *41*(1). https://doi.org/10.1016/0019-
991 1035(80)90156-6
992 Dumoulin, C., Tobie, G., Verhoeven, O., Rosenblatt, P., & Rambaux, N. (2017). Tidal
993 constraints on the interior of Venus. *Journal of Geophysical Research: Planets*.
994 https://doi.org/10.1002/2016JE005249
995 Dziewonski, A. M., & Anderson, D. L. (1981). Preliminary reference Earth model. *Physics of the*
996 *Earth and Planetary Interiors*, *25*(4), 297–356. https://doi.org/10.1016/0031-
997 9201(81)90046-7
998 Efroimsky, M. (2012). TIDAL DISSIPATION COMPARED TO SEISMIC DISSIPATION: IN
999 SMALL BODIES, EARTHS, AND SUPER-EARTHS. *The Astrophysical Journal*,
1000 *746*(2), 150. https://doi.org/10.1088/0004-637X/746/2/150
1001 Evans, S., Taber, W., Drain, T., Smith, J., Wu, H.-C., Guevara, M., Sunseri, R., & Evans, J.
1002 (2018). MONTE: the next generation of mission design and navigation software. *CEAS*
1003 *Space Journal*, *10*(1), 79–86. https://doi.org/10.1007/s12567-017-0171-7
1004 Garate-Lopez, I., & Lebonnois, S. (2018). Latitudinal variation of clouds' structure responsible
1005 for Venus' cold collar. *Icarus*, *314*, 1–11. https://doi.org/10.1016/j.icarus.2018.05.011
1006 Gold, T., & Soter, S. (1971). Atmospheric tides and the 4-day circulation on Venus. *Icarus*,
1007 *14*(1), 16–20. https://doi.org/10.1016/0019-1035(71)90098-4
1008 Goossens, S. J., Lemoine, F. G., Rosenblatt, P., Lebonnois, S., & Mazarico, E. (2017). Venus
1009 Gravity Field Modeling from Magellan and Venus Express Tracking Data. *In Lunar and*
1010 *Planetary Science Conference*, 1984.

Goossens, S. J., Mazarico, E., Rosenblatt, P., Lebonnois, S., & Lemoine, F. G. (2018). Venus Gravity Field Determination Using Magellan and Venus Express Tracking Data. *16th Meeting of the Venus Exploration and Analysis Group (VEXAG)*, 8029.

Goossens, S., Renaud, J. P., Henning, W. G., Mazarico, E., Bertone, S., & Genova, A. (2022). Evaluation of Recent Measurements of Mercury's Moments of Inertia and Tides Using a Comprehensive Markov Chain Monte Carlo Method. *The Planetary Science Journal*, *3*(2), 37. https://doi.org/10.3847/PSJ/ac4bb8

Hensley, S., Campbell, B., Perkovic-Martin, D., Wheeler, K., Kiefer, W., & Ghail, R. (2020). VISAR and VenSAR: Two Proposed Radar Investigations of Venus. *2020 IEEE Radar Conference (RadarConf20)*, 1–6. https://doi.org/10.1109/RadarConf2043947.2020.9266323

Iess, L., Asmar, S. W., Cappuccio, P., Cascioli, G., Marchi, F. D., Stefano, I. di, Genova, A., Ashby, N., Barriot, J. P., Bender, P., Benedetto, C., Border, J. S., Budnik, F., Ciarcia, S., Damour, T., Dehant, V., Achille, G. D., Ruscio, A. D., Fienga, A., … Zannoni, M. (2021). Gravity, Geodesy and Fundamental Physics with BepiColombo's MORE Investigation. *Space Science Reviews*, *217*(1). https://doi.org/10.1007/s11214-021-00800-3

Jacobson, S. A., Rubie, D. C., Hernlund, J., Morbidelli, A., & Nakajima, M. (2017). Formation, stratification, and mixing of the cores of Earth and Venus. *Earth and Planetary Science Letters*, *474*, 375–386. https://doi.org/10.1016/j.epsl.2017.06.023

Jara-Orué, H. M., & Vermeersen, B. L. A. (2011). Effects of low-viscous layers and a non-zero obliquity on surface stresses induced by diurnal tides and non-synchronous rotation: The case of Europa. *Icarus*, *215*(1), 417–438. https://doi.org/10.1016/j.icarus.2011.05.034

Jellinek, A. M. (2002). The influence of interior mantle temperature on the structure of plumes: Heads for Venus, Tails for the Earth. *Geophysical Research Letters*, *29*(11), 1532. https://doi.org/10.1029/2001GL014624

Kamata, S., Matsuyama, I., & Nimmo, F. (2015). Tidal resonance in icy satellites with subsurface oceans: TIDAL RESONANCE IN ICY SATELLITES. *Journal of Geophysical Research: Planets*, *120*(9), 1528–1542. https://doi.org/10.1002/2015JE004821

Kane, S. R., Arney, G., Crisp, D., Domagal-Goldman, S., Glaze, L. S., Goldblatt, C., Grinspoon, D., Head, J. W., Lenardic, A., Unterborn, C., Way, M. J., & Zahnle, K. J. (2019). Venus as a Laboratory for Exoplanetary Science. *Journal of Geophysical Research: Planets*, *124*(8), 2015–2028. https://doi.org/10.1029/2019JE005939

Kaula, W. M. (1966). *Theory of satellite geodesy. Applications of satellites to geodesy*. Dover Publications Inc.

Kervazo, M., Tobie, G., Choblet, G., Dumoulin, C., & Běhounková, M. (2021). Solid tides in Io's partially molten interior: Contribution of bulk dissipation. *Astronomy & Astrophysics*, *650*, A72. https://doi.org/10.1051/0004-6361/202039433

Konopliv, A. S., Banerdt, W. B., & Sjogren, W. L. (1999). Venus Gravity: 180th Degree and Order Model. *Icarus*, *139*(1), 3–18. https://doi.org/10.1006/icar.1999.6086

Lourenço, D. L., Rozel, A. B., Ballmer, M. D., & Tackley, P. J. (2020). Plutonic-Squishy Lid: A New Global Tectonic Regime Generated by Intrusive Magmatism on Earth-Like Planets. *Geochemistry, Geophysics, Geosystems*, *21*(4). https://doi.org/10.1029/2019GC008756

Love, A. E. H. (1911). *Some Problems of Geodynamics*. University Press.

Margot, J.-L., Campbell, D. B., Giorgini, J. D., Jao, J. S., Snedeker, L. G., Ghigo, F. D., & Bonsall, A. (2021). Spin state and moment of inertia of Venus. *Nature Astronomy*, *5*(7), 676–683. https://doi.org/10.1038/s41550-021-01339-7

Mazarico, E., Genova, A., Goossens, S., Lemoine, F. G., Neumann, G. A., Zuber, M. T., Smith, D. E., & Solomon, S. C. (2014). The gravity field, orientation, and ephemeris of Mercury from MESSENGER observations after three years in orbit. *Journal of Geophysical Research: Planets*. https://doi.org/10.1002/2014JE004675

Mazarico, E., Iess, L., Breuer, D., Marchi, F. D., Konopliv, A. S., Hensley, S., & Smrekar, S. (2019). Exploring the Interior of Venus with the VERITAS Gravity Science Investigation. *American Geophysical Union, Fall Meeting 2019, Abstract #P34A-02*.

Milani, A., & Gronchi, G. (2009). *Theory of Orbit Determination*. Cambridge University Press. https://doi.org/10.1017/CBO9781139175371

Navarro, T., Ermakov, A., Bills, B., & Schubert, G. (2023). *Tidal tomography of the venusian atmosphere*. Venus Surface and Atmosphere 2023. https://www.hou.usra.edu/meetings/venussurface2023/pdf/8047.pdf

Nimmo, F. (2002). Why does Venus lack a magnetic field? *Geology*, *30*(11), 987. https://doi.org/10.1130/0091-7613(2002)030<0987:WDVLAM>2.0.CO;2

O'Rourke, J. G., Gillmann, C., & Tackley, P. (2018). Prospects for an ancient dynamo and modern crustal remanent magnetism on Venus. *Earth and Planetary Science Letters*, *502*, 46–56. https://doi.org/10.1016/j.epsl.2018.08.055

Petricca, F., Genova, A., Goossens, S., Iess, L., & Spada, G. (2022). Constraining the Internal Structures of Venus and Mars from the Gravity Response to Atmospheric Loading. *The Planetary Science Journal*, *3*(7), 164. https://doi.org/10.3847/PSJ/ac7878

Renaud, J. P. (2022). *TidalPy* (0.3.5). Zenodo. https://doi.org/10.5281/ZENODO.7017475

Renaud, J. P. (2023). *CyRK - ODE Integrator Implemented in Cython and Numba* (0.4.0). Zenodo. https://doi.org/10.5281/zenodo.7683590

Renaud, J. P., & Henning, W. G. (2018). Increased Tidal Dissipation Using Advanced Rheological Models: Implications for Io and Tidally Active Exoplanets. *The Astrophysical Journal*, *857*(2), 98. https://doi.org/10.3847/1538-4357/aab784

Rivoldini, A., Hoolst, T. V., Verhoeven, O., Mocquet, A., & Dehant, V. (2011). Geodesy constraints on the interior structure and composition of Mars. *Icarus*, *213*(2). https://doi.org/10.1016/j.icarus.2011.03.024

Rolf, T., Steinberger, B., Sruthi, U., & Werner, S. C. (2018). Inferences on the mantle viscosity structure and the post-overturn evolutionary state of Venus. *Icarus*, *313*, 107–123. https://doi.org/10.1016/j.icarus.2018.05.014

Sabadini, R., & Vermeersen, B. (2004). *Global Dynamics of the Earth* (Vol. 20). Springer Netherlands. https://doi.org/10.1007/978-94-017-1709-0

Saito, M. (1974). Some problems of static deformation of the earth. *Journal of Physics of the Earth*, *22*(1), 123–140. https://doi.org/10.4294/jpe1952.22.123

Scarica, P., Garate-Lopez, I., Lebonnois, S., Piccioni, G., Grassi, D., Migliorini, A., & Tellmann, S. (2019). Validation of the IPSL Venus GCM Thermal Structure with Venus Express Data. *Atmosphere*, *10*(10), 584. https://doi.org/10.3390/atmos10100584

Smrekar, S. E., & Sotin, C. (2012). Constraints on mantle plumes on Venus: Implications for volatile history. *Icarus*, *217*(2), 510–523. https://doi.org/10.1016/j.icarus.2011.09.011

Smrekar, S., Hensley, S., Nybakken, R., Wallace, M. S., Perkovic-Martin, D., You, T.-H., Nunes, D., Brophy, J., Ely, T., Burt, E., Dyar, M. D., Helbert, J., Miller, B., Hartley, J.,

Kallemeyn, P., Whitten, J., Iess, L., Mastrogiuseppe, M., Younis, M., … Mazarico, E. (2022). VERITAS (Venus Emissivity, Radio Science, InSAR, Topography, and Spectroscopy): A Discovery Mission. *2022 IEEE Aerospace Conference (AERO)*, 1–20. https://doi.org/10.1109/AERO53065.2022.9843269

Takeuchi, H., & Saito, M. (1972). Seismic Surface Waves. In *Methods in Computational Physics: Advances in Research and Applications* (Vol. 11, pp. 217–295). Elsevier. https://doi.org/10.1016/B978-0-12-460811-5.50010-6

Tapley, B. D., Schutz, B. E., & Born, G. H. (2004). *Statistical Orbit Determination*. Elsevier. https://doi.org/10.1016/B978-0-12-683630-1.X5019-X

Tobie, G., Mocquet, A., & Sotin, C. (2005). Tidal dissipation within large icy satellites: Applications to Europa and Titan. *Icarus*, *177*(2), 534–549. https://doi.org/10.1016/j.icarus.2005.04.006

Wahr, J., Molenaar, M., & Bryan, F. (1998). Time variability of the Earth's gravity field: Hydrological and oceanic effects and their possible detection using GRACE. *Journal of Geophysical Research: Solid Earth*, *103*(B12), 30205–30229. https://doi.org/10.1029/98JB02844

Way, M. J., Del Genio, A. D., Kiang, N. Y., Sohl, L. E., Grinspoon, D. H., Aleinov, I., Kelley, M., & Clune, T. (2016). Was Venus the first habitable world of our solar system? *Geophysical Research Letters*, *43*(16), 8376–8383. https://doi.org/10.1002/2016GL069790

Weller, M. B., & Kiefer, W. S. (2020). The Physics of Changing Tectonic Regimes: Implications for the Temporal Evolution of Mantle Convection and the Thermal History of Venus.

Journal of Geophysical Research: Planets, *125*(1). https://doi.org/10.1029/2019JE005960

Wieczorek, M. A., & Meschede, M. (2018). SHTools: Tools for Working with Spherical Harmonics. *Geochemistry, Geophysics, Geosystems*, *19*(8), 2574–2592. https://doi.org/10.1029/2018GC007529

Xiao, C. (2019). *Replication Data for: Manuscript "Possible Deep Structure and Composition of Venus with Respect to the Current Knowledge from Geodetic Data"* [Data set]. Harvard Dataverse. https://doi.org/10.7910/DVN/7R0DFU

Xiao, C., Li, F., Yan, J., Gregoire, M., Hao, W., Harada, Y., Ye, M., & Barriot, J. (2021). Possible Deep Structure and Composition of Venus With Respect to the Current Knowledge From Geodetic Data. *Journal of Geophysical Research: Planets*, *126*(7). https://doi.org/10.1029/2019JE006243